MRC

Conformational states of human H-Ras detected by high-field EPR, ENDOR, and ^{31}P NMR spectroscopy[†]

Michael Spoerner,[1] Thomas F. Prisner,[2] Marina Bennati,[2] Melanie M. Hertel,[2] Norbert Weiden,[3] Thomas Schweins[4] and Hans Robert Kalbitzer[1]*

[1] Institute for Biophysics and Physical Biochemistry, University of Regensburg, Germany
[2] Institute for Physical and Theoretical Chemistry and Centre for Biomolecular Magnetic Resonance, Johann-Wolfgang-Goethe-University, Frankfurt a. M., Germany
[3] Institute for Physical Chemistry, University of Darmstadt, Germany
[4] QIAGEN GmbH, Hilden, Germany

Ras is a central constituent of the intracellular signal transduction that switches between its inactive state with GDP bound and its active state with GTP bound. A number of different X-ray structures are available. Different magnetic resonance techniques were used to characterise the conformational states of the protein and are summarised here. ^{31}P NMR spectroscopy was used as probe for the environment of the phosphate groups of the bound nucleotide. It shows that in liquid solution additional conformational states in the GDP as well as in the GTP forms coexist which are not detected by X-ray crystallography. Some of them can also be detected by solid-state NMR in the micro crystalline state. EPR and ENDOR spectroscopy were used to probe the environment of the divalent metal ion (Mg^{2+} was replaced by Mn^{2+}) bound to the nucleotide in the protein. Here again different states could be observed. Substitution of normal water by ^{17}O-enriched water allowed the determination of the number of water molecules in the first coordination sphere of the metal ion. In liquid solution, they indicate again the existence of different conformational states. At low temperatures in the frozen state ENDOR spectroscopy suggests that only one state exists for the GDP- and GTP-bound form of Ras, respectively. Copyright © 2005 John Wiley & Sons, Ltd.

KEYWORDS: EPR; ENDOR; ^{31}P NMR; Ras; conformational states

INTRODUCTION

Small guanine nucleotide-binding proteins, like the protein product of the protooncongene ras (rat sarcoma) (Ras), act as molecular switches in cellular signalling pathways controlling cell proliferation and differentiation.[1] In the inactive state, GDP is tightly bound to the Mg^{2+} ion in the active site of the protein. Guanine nucleotide exchange factors (GEFs) catalyse the dissociation of GDP from Ras and thus allow the uptake of free cellular guanosine-5′-triphosphate (GTP) (Fig. 1). In this (active) state of the complex, it can interact with different effector molecules such as Raf-kinase or RalGDS, which transmit signals to the next downstream component in the signalling pathway. GTP is hydrolysed to GDP and inorganic phosphate in the catalytic cycle. The rather slow intrinsic hydrolysis rate of Ras can be enhanced up to 5 orders of magnitude by specific GTPase-activating proteins (GAPs), which therefore act as a 'fast switch off' mechanism for the signal transfer cascade.[2]
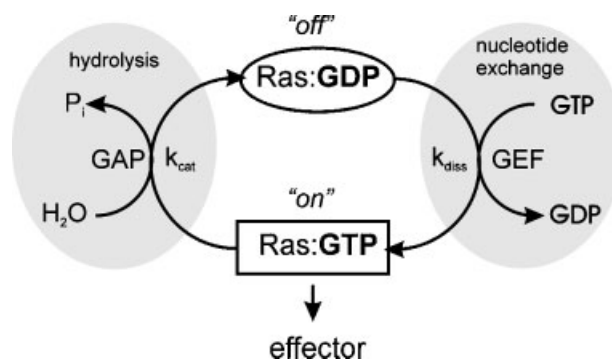
Figure 1. Signal transduction by guanine nucleotide-binding proteins of the Ras superfamily. (GEF: guanine nucleotide exchange factor, GAP: GTPase-activating protein).

Crystal structures of the active as well as the inactive state are available at very high resolution;[3–7] nevertheless, fundamental steps in the catalytic reaction are still under debate and are not fully understood. From the crystal structure, one specific water molecule in the pocket of the active site that is assumed to be responsible for nucleophilic attack at the γ-phosphate of the GTP nucleotide could be localised.[8] It was suggested that an arginine finger of the RasGAP plays a role in the stabilisation and energetic

optimisation of the transition state for the hydrolysis reaction.[9] From extensive NMR,[10–15] FTIR,[16–19] Raman,[20] and MD[21–23] studies, it seems clear that conformational dynamics at the active site play an important role for the rate of the hydrolysis reaction and for the interaction with effectors. EPR spectroscopy,[24–26] especially pulsed,[27–30] and high-field[31–33] methods have also been used to investigate structural and dynamical properties of the two states of the protein complex in the active site, with the natural diamagnetic Mg^{2+} ion substituted by the paramagnetic Mn^{2+} ion ($S = 5/2, I = 5/2$). The X-ray structure of the Mn^{2+} complex and also the enzymatic activity have been shown to be very similar to the natural Mg^{2+} complexes.[34]

The results derived by these different methods are to a large extend similar, but especially structural details of the active site of the protein in different functional states are still under debate. The active site of the protein contains motifs within the P−loop (amino acids 10–17), the switch I (amino acids 30–36), and the switch II (amino acids 60–72) region, which are involved in the coordination of the metal ion as well as the phosphates of the nucleotide by specific side chain and main chain interactions.

It was shown by ^{31}P NMR spectroscopy that the switch I region containing the effector binding site exists in solution in at least two different conformational states.[10,13–15] This equilibrium was not detected by X-ray crystallography. These different states of the protein complex are rather similar in terms of free energies and may be called 'excited states' of the protein. Their existence is probably a consequence of the fact that the Ras protein has to interact with a variety of different effectors, GAPs and GEFs in the active state, and thus must be able to adopt slightly different conformations to account for the differences in interaction sites.

In the present paper, we will summarise and combine the spectroscopic data from ^{31}P NMR and Mn^{2+} EPR and ENDOR investigations on a variety of different Ras−nucleotide complexes that were recorded for elucidating the structural properties in the active site of Ras.

MATERIALS AND METHODS

Protein purification
Wild type and mutants of human H-Ras (1–189) were expressed in *E. coli* strain CK600K with ptac vector plasmids and purified as described before.[35] Ras•Mg^{2+} complexes with guanosine-5'-(β,γ-imido)triphosphate (GppNHp), guanosine-5'-(β,γ-methyleno)triphosphate (GppCH$_2$p), or guanosine-5'-O-(3-thiotriphosphate) (GTPγS) were generated by treatment of Ras•GDP (in 50 mM Tris/HCl pH 7.6, 200 mM (NH$_4$)$_2$SO$_4$, 2 mM 1,4-dithioerythritol (DTE)) with alkaline phosphatase in the presence of twofold excess of the GTP analog overnight at 5 °C. Afterwards, free nucleotide, salt, and enzymes were separated from the protein by gel filtration. The Ras-binding domains of human cRaf-1 (Ras-binding domain of Raf-kinase (Raf-RBD), amino acid 51–131) or RalGDS-RBD (amino acid 11–97) were expressed in *E. coli* as glutathion-*S*-transferase (GST) fusion protein. The complex was purified by GSH column and eluted after cleavage with

thrombin. Finally, the Ras-binding domains (RBDs) were purified by gel filtration.[36,37]

Sample preparation for NMR spectroscopy
Typically, 1 mM Ras bound to Mg^{2+}•GDP, Mg^{2+}•GppNHp, Mg^{2+}•GppCH$_2$p, or Mg^{2+}•GTPγS was dissolved in 40 mM HEPES/NaOH pH 7.4, 10 mM MgCl$_2$, 150 mM NaCl, 2 mM DTE, and 0.1 mM 2,2-dimethyl-2-silapentane-5-sulfonate (DSS) in 5% D$_2$O, 95% H$_2$O. For binding studies, a solution of 5−7 mM Raf-RBD contained in the same buffer was added in appropriate amounts to the samples.

Sample preparation for EPR and ENDOR spectroscopy.
Ras•Mn^{2+}•GDP/GppNHp was prepared by incubation of 100 µM Ras•Mg^{2+}•GDP/GppNHp in 50 mM Tris/HCl, pH 7.6, 5 mM DTE, 300 mM (NH$_4$)$_2$SO$_4$, and 200 mM MnCl$_2$ overnight at 278 K. Salts and excess MnCl$_2$ were separated by size exclusion chromatography in 40 mM HEPES/NaOH, pH 7.4, and 2 mM DTE, treated with chelating resin (Chelex 100). Samples with H$_2$^{17}O were obtained by lyophilising frozen samples and dissolving the protein in the same amount of H$_2$^{17}O (46.3%, Isotec). About 5 µl of the sample was loaded in quartz capillary tubes for W-band (0.9 mm outer diameter), frozen in liquid nitrogen, and inserted into the pre-cooled cryostat at about 100 K. There is no indication of free manganese in the solutions and it is not to be expected from the preparation procedure, which effectively removes small compounds as free nucleotides, as can be shown by phosphorus NMR. Free manganese results in EPR spectra with typical linewidths and intensity distributions that differ from those of bound manganese. An analysis of the EPR spectra shows that the free manganese concentration is <5% of the total manganese in the sample.

NMR spectroscopy
^{31}P NMR spectra were recorded with a Bruker DRX-500 NMR spectrometer operating at 202 MHz. Measurements were performed in a 10-mm probe using 8-mm Shigemi sample tubes at various temperatures. Seventy degree pulses together with a total repetition time of 7 s were used. Protons were decoupled during data acquisition by a GARP sequence[38] with a strength of the B_1-field of 830 Hz. A Ξ-value of 0.4048073561 reported by Maurer and Kalbitzer[39] was used, which corresponds to 85% external phosphoric acid contained in a spherical bulb. Temperature was controlled by using the line separation (methylene-hydroxyl) of external ethylene glycol.[40] Thus, the absolute accuracy of the temperatures given in this paper is better than ±0.5 K.

^{31}P longitudinal relaxation time T_1 were measured at 278 or 293 K with an inversion recovery sequence using a delay of 22 s between two scans. The signal integrals obtained were fitted by a three-parameter fit to the equation:

$$M_z(t) = M_0 + (M_z(0) - M_0)e^{-\frac{t}{T_1}}$$

where $M_z(t)$ is the z-magnetisation (signal integral) at time t, and M_0 is the magnetisation in thermal equilibrium. Protons

were decoupled during magnetisation recovery by a GARP[38] sequence.
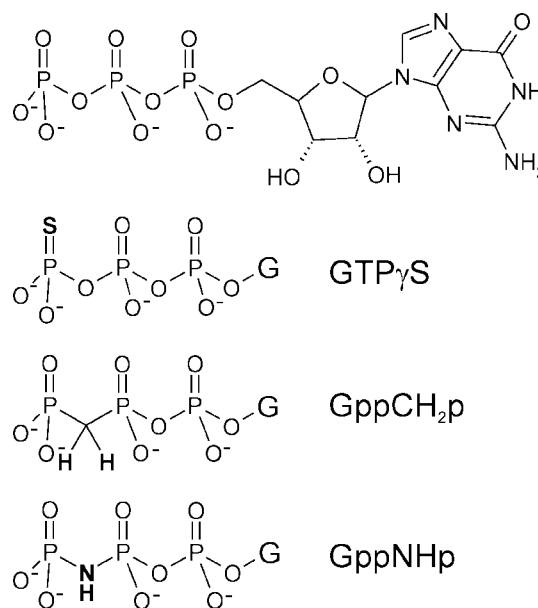
EPR and ENDOR spectroscopy

W-band EPR experiments were performed with a home-built EPR spectrometer or a Bruker E680 spectrometer equipped with a home-built ENDOR probe. In all field-swept cw-EPR-spectra, the modulation amplitude was kept well below the width of any observed structure (typically: S-band 15 G; X-band 10 G; W-band 1 G; G-band 0.2 G). Davies ENDOR spectra were typically acquired with a pulse sequence $(\pi - RF - \pi/2 - \pi)$ consisting of selective pulses, with typical $\pi/2$ pulse lengths around 50 ns for the $S = 5/2$ of the Mn^{2+}. The sequence was employed to detect couplings larger than approximately 4–5 MHz, as is to be expected in the ^{17}O or ^{31}P spectra. Mims ENDOR $(\pi/2 - \tau - \pi/2 - F - \pi/2)$ was rather used to detect weak hyperfine couplings (hfc)s as encountered in the ^{13}C spectra. The length of the RF pulse varied for the different nuclei and was optimised for a maximum ENDOR effect. Detailed experimental parameters of the ^{17}O spectra are given in Fig. 7 and may be looked up in Bennati *et al.*[41] for the ^{13}C and ^{31}P spectra.

RESULTS AND DISCUSSION

Characterisation of Ras–nucleotide complexes by ^{31}P NMR spectroscopy

^{31}P NMR spectroscopy allows probing of the conformational states of nucleotide-binding proteins such as Ras-related proteins, which depend on the type of nucleotide present in the active centre. Also, we can investigate the effect of different mutations in Ras proteins on the structural situation and the dynamic properties in the active site. In principle, whenever chemical shift changes are visible, they indicate that there is a change in the environment of the phosphorus nuclei. Main mechanisms in chemical shift changes are conformational strain and electric field effects polarising the oxygens of the phosphate groups. In addition to these direct effects, long-range effects may occur, which can be caused by a structure-dependent change of the anisotropy of the magnetic susceptibility, with the ring current effects as the most dominant contribution.

^{31}P NMR investigations were performed on Ras in the inactive GDP-bound state[33] as well as in complex with different slowly hydrolysing GTP analogs (Scheme 1) representing the active state of Ras.[10,13–15] In general, more than one set of ^{31}P NMR lines for the bound nucleotide is detected, indicating the existence of more than one structural state (Table 1). This is true for the nucleoside diphosphate as well as for the triphosphate complexes. In the active state of Ras(wt), the GTP analog bound influences the conformational equilibria. In complex with the GTP analog GppNHp or GppCH$_2$p, Ras wild type exists in two interconverting conformational states with exchange rates in the millisecond timescale at room temperature. The equilibrium constants $K_{12} = [2]/[1]$ are 1.9 for the Ras•Mg^{2+}•GppNHp complex and 2.0 for the complex Ras(wt)•Mg^{2+}•GppCH$_2$p. In contrast, the ^{31}P NMR spectrum of Ras(wt) indicates the

Scheme 1. Sketches of GTP and commonly used GTP analogs. The abbreviations used here are indicated. G, guanosine; GTP, guanosine-5′-triphosphate; GppCH$_2$p, guanosine-5′-(β,γ-methyleno)triphosphate; GppNHp, guanosine-5′-(β,γ-imido) triphosphate; GTPγS, guanosine-5′-O-(3-thiotriphosphate). The protonation state shown corresponds to the high pH conditions and is also expected in the protein-bound state.

existence of predominantly one state when it is bound to the GTP analog GTPγS (Fig. 2, bottom spectra) or to GTP.[10]

In addition to chemical shifts, relaxation times are typical NMR parameters that characterise the system. For protein-bound nucleotides, only a few phosphorus relaxation data were published in the past. Guanine nucleotides complexed with Ras represent a well-defined model systems to obtain such phosphorus NMR data. The phosphorus longitudinal relaxation times are rather long. The conformational states in the complexes with Ras are in a dynamical equilibrium. In the nucleoside triphosphate complexes, the exchange correlation times are in the millisecond timescale.[10,15] Thus, when more than one state exists, the non-selective inversion recovery experiment measures the averaged T_1 for the two states (Table 2). Since, in general, the Ras proteins exist in a dynamical equilibrium between more than one state, the exchange contribution is usually very large. The exchange contribution can be removed by a simulation of the ^{31}P NMR spectra recorded at different temperatures using the complete density matrix formalism.[10,15] These T_2 relaxation times are given in Table 2.

MAS solid-state ^{31}P NMR experiments were performed on single crystals[42] as well as on powders of micro crystals of Ras–nucleotide complexes.[43] The MAS solid-state NMR experiments indicate that the different conformational states of the Ras•Mg^{2+}•GppNHp complex exist also in the crystal, although they were not seen in the electron density map by X-ray diffraction. In the well-resolved structure (0.135 nm) of H-Ras(wt)•Mg^{2+}•GppNHp[5], the electron density map of the environment of the nucleotide is well defined and does not show anomalies of the B-factors within the amino acids of

Table 1. ^{31}P chemical shifts and conformational states of Ras wild type complexed with different nucleotides[a]

Ras(wt) complex	α-Phosphate		β-Phosphate		γ-Phosphate		K_{12}
	δ_1 (ppm)	δ_2 (ppm)	δ_1 (ppm)	δ_2 (ppm)	δ_1 (ppm)	δ_2 (ppm)	
Ras•Mg^{2+}•GDP[b]	−10.68		−2.00	−2.15			0.31
Ras•Mg^{2+}•GTPγS		−11.30		−16.67		37.01	>10
Ras•Mg^{2+}•GppNHp[c]	−11.20	−11.70	−0.25		−2.59	−3.32	1.9
Ras•Mg^{2+}•GppCH$_2$p[c]	−12.37	−13.26	19.54		8.59	8.20	2.0
Ras•Mg^{2+}•GTP[d]		−11.77		−14.97		−7.99	>10
Ras•Mg^{2+}•GTPγS•Raf-RBD		−11.19		−16.55		36.85	
Ras•Mg^{2+}•GppNHp•Raf-RBD[c]		−11.55		−3.50		−0.22	
Ras•Mg^{2+}•GppCH$_2$p•Raf-RBD[c]		−13.07		19.60		7.90	

[a] Data were recorded at various temperatures. The shifts actually given were taken from spectra recorded at 278 K for Ras complexed with GTP and its analogs and at 298 K for Ras complexed GDP. The estimated error is ±0.05 ppm. The equilibrium constant K_{12} between state 1 and 2 is calculated from integrals of the γ-phosphate resonances (GTP and analogs) or the β-phosphate resonance (GDP) defined by $K_{12} = k_{12}/k_{21} = [2]/[1]$. State 1 and state 2 are two conformational states of the Ras−nucleotide complexes with different chemical shifts. In the Ras•Mg^{2+}•GDP complexes, state 1 is defined as the state in which the β-phosphate resonance is shifted downfield relative to state 2. In Ras complexed to Mg^{2+}•GppNHp or Mg^{2+}•GppCH$_2$p complexes, the resonances corresponding to state 1 are shifted downfield relative to that of state 2 and state 2 is associated with the effector binding state.
[b] Data were taken from Rohrer et al.[33] Note that states 1 and 2 in the GDP form do not necessarily correspond to the states observed in the GTP form.
[c] Data were taken from Spoerner et al.[15] The chemical shifts are slightly different (δ ppm differences <0.16 ppm) from those reported by Geyer et al.[10] owing to differences in the referencing method (direct external referencing to 85% phosphoric acid in a capillary).
[d] Data were taken from Geyer et al.[10] using a slightly different referencing method (see 'c' in preceding text).

switch I region, whereas in amino acids 60 to 67 of switch II significantly increased B-factors for the atoms are obtained.

Furthermore, the equilibrium constant as well as the temperature dependence of the exchange are rather similar to the values obtained in liquid state. Solid-state NMR spectroscopy on single crystals of Ras showed that the principal axis of the chemical shift tensor of the α-phosphate group differs by more than 20° in the two states.[42] The spectroscopic parameters obtained in the crystalline state for Ras(wt)Mg^{2+}•GppNHp and Ras(wt)Mg^{2+}•GppCH$_2$p are summarised in Table 3. It was not possible to get data of a micro crystalline Ras•Mg^{2+}•GTPγS sample since this GTP analog becomes hydrolysed during the time necessary for crystallisation.

^{31}P NMR spectroscopy of Ras−effector complexes

Binding of the Ras-binding domains (RBD) of effectors to Ras leads to ^{31}P NMR spectra that have similar but not identical chemical shifts to those assigned to state 2 of Ras•Mg^{2+}•GppNHp (Fig. 2(c), upper spectrum).[10,13,14,45–47] This indicates that the conformation of Ras in the complex is similar to state 2 of free wild-type Ras. The same is true for Ras(wt)•Mg^{2+}•GppCH$_2$p[15] (Fig. 2(b), upper spectrum). In contrast, binding of Raf-RBD to Ras(wt)•Mg^{2+}•GTPγS leads only to a broadening of the resonances and not to a change in the chemical shift values (Fig. 2(a), upper spectrum). This indicates that Ras(wt)•Mg^{2+}•GTPγS exists predominantly in state 2 in solution even when it is not bound to an effector molecule. The corresponding chemical shift values are summarised in Table 1.

EPR spectroscopy of Ras−nucleotide complexes in liquid solution

As with other nucleotide-binding proteins, the divalent Mg^{2+} ion can be substituted by the paramagnetic Mn^{2+} ion ($S = 5/2, I = 5/2$). From the results derived by X-ray crystallography, the structure seems to be unchanged by the exchange of the metal ion. The affinity of Mg^{2+} to Ras bound to the fluorescent analog mantGppNHp or mantGDP is in the range of 3 μM as determined by using the Mg^{2+} dependence of the observed dissociation rates at 298 K in the same buffer as that used for the EPR and NMR experiments shown here.[13,48] An increased affinity and an increased enzymatic activity are usually observed for enzymes using GTP or ATP as substrates when Mg^{2+} is replaced by Mn^{2+}. This means that the divalent ion itself is involved in the catalytic process. The intrinsic hydrolysis activity is increased by a factor of 5 in the manganese-bound RasGTP complex.[34] GTP hydrolysis in Ras most probably follows the substrate-assisted catalysis mechanism published by Schweins et al.[49] In this theory, the experimentally determined increase of the apparent pKa value of the γ-phosphate by substitution of the coordinated Mg^{2+} ion by a Mn^{2+} ion would directly lead to an enhancement of the hydrolysis reaction.

With the paramagnetic metal ion, the local structure in the vicinity of the metal centre can be studied in detail by EPR spectroscopy and information complementary to that obtained by ^{31}P NMR spectroscopy of the bound nucleotide can be acquired.

A possibility to simplify the analysis of complex biological systems containing manganese ions is the use of high magnetic fields since the contributions to the linewidths by the zero-field splitting tensor decrease proportionally
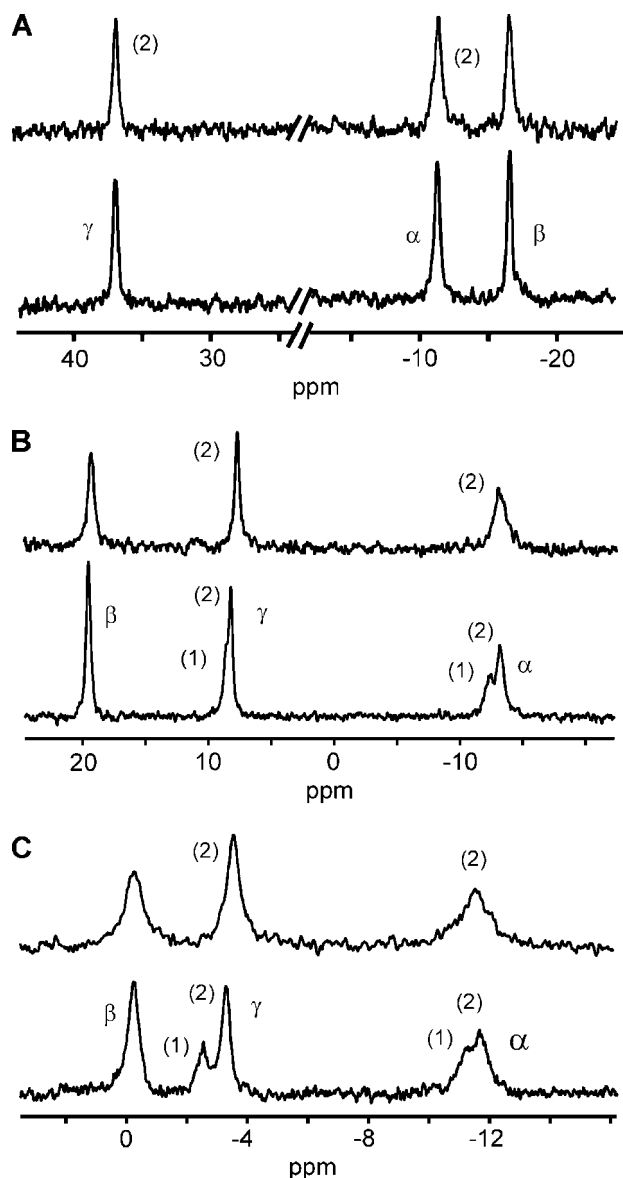
Figure 2. Proton decoupled ^{31}P NMR spectra of wild-type Ras bound to different GTP analogs in the absence of and in the presence of Raf-RBD. The samples initially contained 1 mM (A) Ras•Mg^{2+}•GTPγS (bottom), (B) Ras•Mg^{2+}•GppCH$_2$p (bottom), (C) Ras•Mg^{2+}•GppNHp (bottom) in 40 mM HEPES/NaOH pH 7.4, 150 mM NaCl, 10 mM MgCl$_2$, 2 mM DTE and 0.1 mM DSS in 5% D$_2$O, 95% H$_2$O, respectively. The upper spectra of (A), (B), and (C) represent the corresponding Ras–nucleotide complex in the presence of 2.5-fold excess of Raf-RBD. 1600–2400 FIDs were summarised. Data were recorded at 278 K. Data are filtered by an exponential function, which leads to an additional line broadening of 15 Hz. The assignments of the resonances corresponding to the α-, β-, γ-phosphate group, indicated with α, β, γ were determined by a ^{31}P–^{31}P NOESY experiments.[15] Note that the ppm scales as well as the spectral width are different for the spectra of each Ras–nucleotide complex. The resonances corresponding to the conformational states (state 1 and 2) are indicated.

to the magnetic field. This is shown in Fig. 3. At W-band frequencies (95 GHz, 3.4 T), the contribution of the zero-field

splitting is already rather small so that other contributions to the inhomogeneous linewidth, such as hyperfine couplings, dominate.

An elegant method to study the water molecules in the first coordination shell of the metal ion is the replacement of normal water by ^{17}O-enriched water.[24] ^{17}O has a nuclear spin $I = 5/2$. A ^{17}O isotope enrichment of approximately 50% is optimal for these studies. The observation of the inhomogeneous line broadening by the ^{17}O hyperfine coupling allows the determination of the number of water molecules in the first coordination shell. The method relies critically on the feasibility to spectrally separate the peak from Mn^{2+} ions with no ^{17}O in the ligand sphere from the peak arising from Mn^{2+} ions with ^{17}O bound in the coordination sphere (Fig. 4) in the first-derivative cw-EPR signal. In this case, the intensity ratio of these two peaks allows to sensitively determine the water coordination number. This method has been applied by several groups[31,33,50] to different Ras–nucleotide complexes. The values obtained together with the isotropic part of the ^{17}O hfc constant are summarised in Table 4. The data analysis assumed, in all cases, a unique integer number of water ligands in the first ligand sphere of the hexacoordinated metal ion. The solution data indicated that in solution H-Ras(wt)•Mg^{2+}•GDP and H-Ras(T35S)•Mg^{2+}•GDP contain only three water ligands of manganese, whereas H-Ras(T35A)•Mg^{2+}•GDP and the GDP complex of oncogenic mutants of H-Ras with mutations in position 12 are characterised by four water ligands (Table 4). This assumption need not necessarily to be true if the mixture of different conformational states, as shown by ^{31}P NMR spectroscopy for Ras(wt), Ras(T35S), and Ras(T35A) bound to Mg^{2+}•GDP, and Ras(wt)•Mg^{2+}•GppNHp[10,33] (Table 1) directly correlates with the number of water ligands. Indeed, a slightly better fit of the experimental data could be achieved for the Ras(T35A) mutant assuming a mixture of three to four bound water molecules.

In the frozen state, the intrinsic linewidth is increased compared to the liquid solution, probably by anisotropic hyperfine interactions of close nuclei (^1H, ^{31}P, ^{14}N) (Fig. 4(d)). This effect is strong enough to lose the spectral resolution of the above-mentioned peaks, so that only a line broadening by ^{17}O isotope labelling can be observed. This strongly reduces the accuracy in the determination of the water coordination number. In the frozen state, slightly better results were obtained by this method assuming four water ligands for the GDP complexes and two water ligands for the GppNHp complex (Table 4).

The isotropic part of the ^{17}O hfc constant determined by these simulations of the HF cw-EPR data are in good agreement with the values determined much more accurately by the ENDOR experiments, which are described in the following text.

Complexes of Ras with a number of non-hydrolysable analogs of the GTP nucleotide (GppNHp, GppCH$_2$p, GTPγS) have been measured by cw-EPR at 95 GHz (Fig. 5). Compared to the GDP complexes, the peak-to-peak linewidth of all these complexes approximately doubles at room temperature (Fig. 5(d)). Further, line broadening is also observed

Table 2. Phosphorus relaxation times in different Ras−nucleotide complexes[a]

| | | Relaxation times T_1 (s) of the resonances of | | | | | |
| | | α-Phosphate | | β-Phosphate | | γ-Phosphate | |
Ras(wt) complex	T (K)	(1)	(2)	(1)	(2)	(1)	(2)
Ras•Mg^{2+}•GTPγS	278		2.4 ± 0.4		2.9 ± 0.4		4.4 ± 0.7
Ras•Mg^{2+}•GppNHp[b]	278		4.5 ± 0.4		5.3 ± 0.3		5.6 ± 0.4
Ras•Mg^{2+}•GppCH$_2$p[b]	293		1.5 ± 0.1		2.9 ± 0.2		3.2 ± 0.2

| | | Relaxation times T_2 (ms) of the resonances of | | | | | |
| | | α-Phosphate | | β-Phosphate | | γ-Phosphate | |
		(1)	(2)	(1)	(2)	(1)	(2)
Ras•Mg^{2+}•GppNHp[b]	278	5.8	3.9	4.8	4.8	4.1	7.1
Ras•Mg^{2+}•GppCH$_2$p[b]	278	4.2	4.0	6.4	6.4	3.8	5.2

[a] The T_1 times were determined by a proton decoupled, non-selective inversion recovery sequence. Since non-selective pulses were used and $\tau_{ex} \ll T_1$, the T_1 relaxation times of states 1 and 2 are averaged in the GppNHp and the GppCH$_2$p complex. Note that T_1 relaxation of the GppCH$_2$p complex was determined at 293 K. The T_2 times were calculated by lineshape analysis based on the full density matrix formalism. Exchange contributions were removed in this way. The estimated error for the T_2 values given is ±0.5 ms.
[b] Data from Spoerner et al.[15] Note that the values given differ somewhat from those given by Geyer et al.[10] since the absolute temperature was controlled independently and the new assignment of the signals were considered.

Table 3. NMR spectroscopic parameters of crystalline Ras(wt)·Mg^{2+}·GppCH$_2$p and Ras(wt)Mg^{2+}•GppNHp[a]

| | Ras(wt)•Mg^{2+}•GppCH$_2$p | | | | |
Phosphate group	δ_{xx} (ppm) (±0.1 ppm)	δ_{yy} (ppm) (±3 ppm)	δ_{zz} (ppm) (±0.1 ppm)	T_{IS} (μs) (±10%)	$T_{1\rho}^{H}$ (ms) (±10%)
α	71	32	−143	124	16
β	95	19	−57	67	15
γ	−43	−26	90	67	14

| | Ras(wt)•Mg^{2+}•GppNHp | | | | |
Phosphate group	δ_{xx} (ppm) (±0.1 ppm)	δ_{yy} (ppm) (±3 ppm)	δ_{zz} (ppm) (±0.1 ppm)	T_{IS} (μs) (±10%)	$T_{1\rho}^{H}$ (ms) (±10%)
α	99	8	−142	171	5.6
β	99	11	−110	111	9.0
γ_2	−67	−38	94	198	6.7
γ_1	79	7	−92	n.m.	n.m.

[a] Data were calculated using the values published by Iuga et al.[43] measured at 273 K. $T_{1\rho}^{H}$ and T_{IS} were determined from the CP buildup curves, i.e., the dependence of the intensity, I_{CP}, of the ^{31}P {^{1}H} CP MAS NMR signal upon the contact time: $I_{CP} \sim (1 - \lambda)^{-1} \times (1 - \exp[-(1 - \lambda)t/T_{IS}]) \times \exp[-t/T_{1\rho}^{H}]$ with $\lambda = T_{IS}/T_{1\rho}^{H}$ (see Ref. 44).

in these complexes in the frozen state at 20 K (data not shown). The same observation has been reported earlier for GppNHp by Bellew et al.[31] This increase in linewidths seems to be a more general feature of small GTPases: at least in elongation factor EF-Tu the manganese linewidth of the GTP complex is also about a factor of 2 larger than that of the GDP complex.[51] Because of these increased linewidths, the accurate determination of the water coordination number of these complexes is much more difficult, but a preliminary data analysis shows that all of the complexes (besides the complex with the GTPγS nucleotide) were compatible with a simulation assuming two water ligands.

Effector proteins stabilise conformational state 2 at the active site of Ras•Mg^{2+}•GppNHp complexes, as has been shown by ^{31}P NMR spectroscopy.[10,13,14,45−47] Therefore, we have also measured by cw HF-EPR the complexes of Ras•Mn^{2+}•GppNHp with the RBD of the effector protein Raf-kinase[36] and RalGDS.[37] No significant changes in the cw-EPR lineshape could be observed by the addition of these effectors to the Ras(wt)•Mn^{2+}•GppNHp complex (Fig. 6).
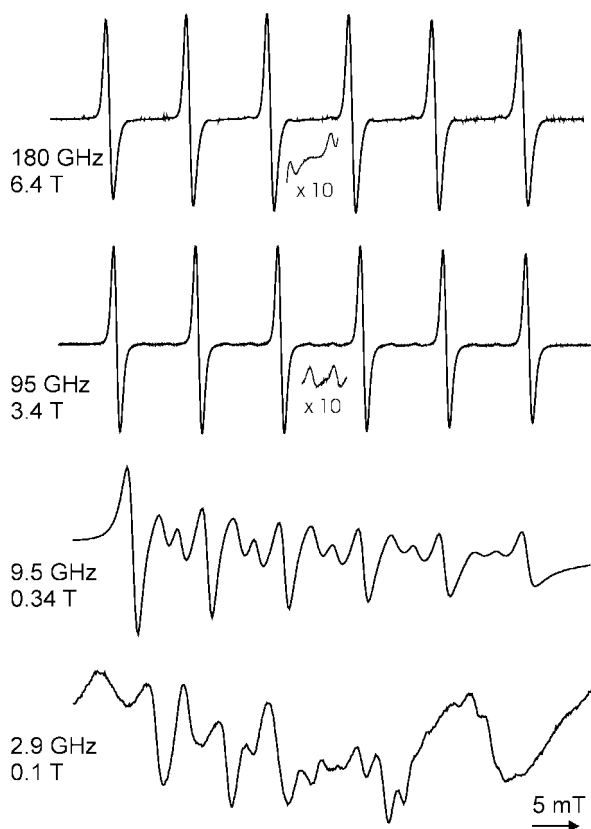
Figure 3. EPR spectra of Ras(wt)•Mn^{2+}•GDP at various magnetic fields. The sample contained 1 mM Ras(wt)•Mn^{2+}•GDP in 40 mM HEPES/NaOH pH 7.4, 2 mM DTE. The magnetic field and the microwave frequencies are indicated. The 2.9 GHz spectrum was recorded at 10 K, and the other spectra were recorded at 20 K.

HF-ENDOR of Ras−nucleotide complexes in frozen solution

Determination of the Mn^{2+}-^{17}O hfc

All cw-EPR studies performed to count the number of the coordinated water molecules in the GDP and GTP complexes with Ras had been based on the analysis of the hyperfine broadening produced by the H_2O–^{17}O nuclei on the Mn^{2+} EPR lines; however, the precise value of the ^{17}O hyperfine coupling has been unknown. High-field ENDOR spectroscopy represents the most direct method to measure this hfc. The ^{17}O Davies ENDOR spectra of the wild-type Ras and Ras(G12V)•Mn^{2+}•GDP complexes[41] are illustrated in Fig. 7.

The spectra clearly indicate a structured doublet centered at the expected ^{17}O nuclear Zeeman frequency (19.5 MHz) and split by ≈8 MHz, which was assigned to the ENDOR lines arising from the EPR $m_S = \pm1/2$ manifolds. The spectra were analysed with an ENDOR simulation program described previously[52] and the results gave one set of tensor parameters: $A_x = -6.27$ MHz, $A_y = -6.86$ MHz, $A_z = -10.10$ MHz, $Q_x = -0.238$ MHz, $Q_y = 0.238$ MHz, $Q_z = 0$ and the Euler angles $\alpha = 15°$, $\beta = 35°$, $\gamma = 0$. Here, the Euler angles represent the mutual orientation of the hyperfine and the quadrupole tensor. The error of the simulated tensor components was estimated to be
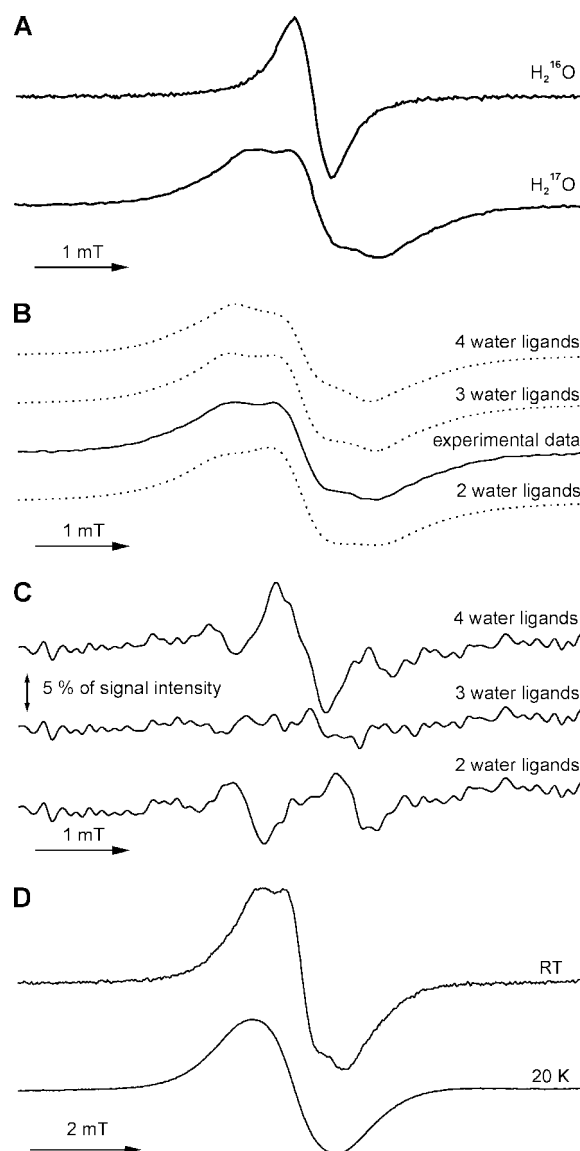

Figure 4. The effect of ^{17}O-enrichment of water on the EPR spectrum of Ras(wt)•Mn^{2+}•GDP. (A)–(D) W-band spectra were recorded on a solution containing approximately 1 mM Ras(wt)•Mn^{2+}•GDP, 40 mM HEPES/NaOH pH 7.4, and 2 mM DTE. Only the lowest-field manganese hyperfine transition is shown. (A) Comparison between the sample in $H_2{}^{16}O$ or in $H_2{}^{17}O$ enriched (46.3%) solution measured at 297 K. (B) Protein sample in $H_2{}^{17}O$ enriched water. The solid line corresponds to the experimental spectrum and the broken lines correspond to the fit of the data with different numbers N of water ligands in the first coordination sphere. The zero-field parameter E was close to zero in all simulations; in the limits of error, $E = 0$ mT can be assumed. The best fit was obtained with $N = 3$, the zero-field splitting parameter $D = 13.6$ mT, and the ^{17}O-^{55}Mn SHF coupling $a = 0.274$ mT. (C) Residuals assuming different numbers N of water ligands of the metal ion. (D) Same sample as in (A) but measured at room temperature and 20 K.

approximately ±5%. The sign of the hfc was obtained from the asymmetry of the ENDOR spectra[41] according to Epel *et al.*[53] The hfc and quadrupole tensor components were
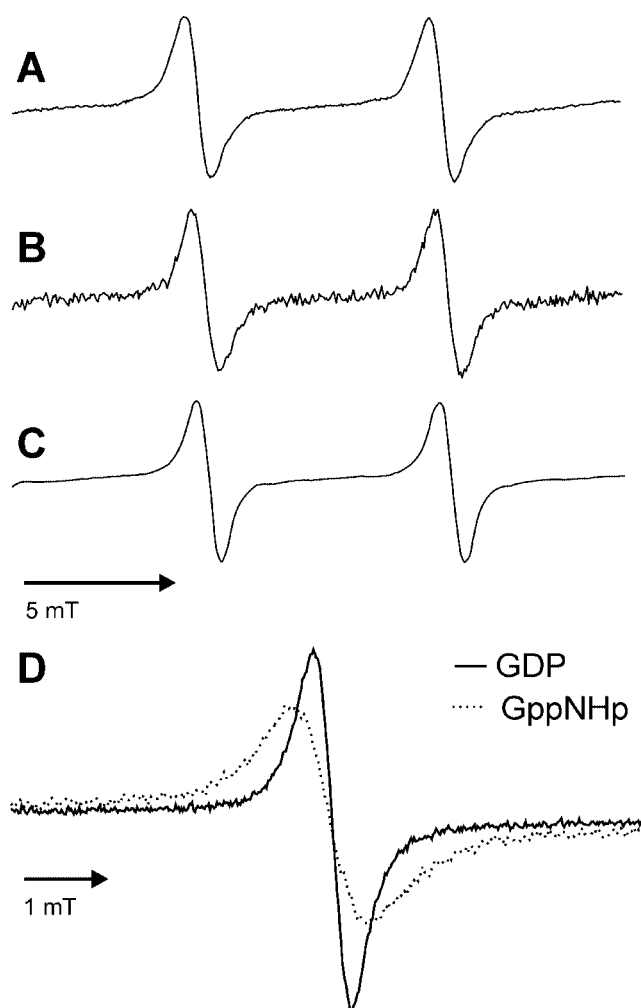
Figure 5. W-band spectra of complexes of Ras(wt) with different Mn^{2+}-nucleotide complexes. Spectra were recorded at 297 K at 95 GHz on approximately 1 mM Ras solution in 40 mM Hepes/NaOH pH 7.4, 2 mM DTE. The two low-field manganese hyperfine transitions are shown. The samples contained 1 mM Ras(wt)•Mn^{2+}•GTPγS (A), 0.8 mM Ras(wt)•Mn^{2+}•GppCH$_2$p (B), and 1 mM Ras(wt)•Mn^{2+}•GppNHp (C). Only the two low-field lines are shown. (D) Overlay of the lowest-field hyperfine line of 1 mM Ras(wt)•Mn^{2+}•GDP and Ras(wt)•Mn^{2+}•GppNHp.

Figure 6. W-band spectra of Ras•Mn^{2+}•GppNHp complexed with effectors. Spectra were measured at 297 K at 95 GHz in 40 mM HEPES/NaOH pH 7.4, 2 mM DTE. The two low-field manganese hyperfine transitions are shown. The samples initially contained 1 mM Ras(wt)•Mn^{2+}•GppNHp (A) in complex with Raf-RBD (B), and in complex with RalGDS-RBD (C). Note that in (B) and (C) the Ras concentration was somewhat lower because of dilution by adding the effector-RBD solution.

found to be very similar to the ones reported by Tan *et al.*[54] for a Mn^{2+} aquo complex. The straightforward interpretation nicely illustrated the great advantages of ENDOR at high fields, where spectra become symmetric around the nuclear Zeeman frequency and contributions of different low gamma nuclei do not overlap.

The principal values of the ^{17}O hyperfine tensor lead to an isotropic hfc of -7.74 MHz or -0.276 mT, with all coupled ^{17}O nuclei being magnetically equivalent within the ENDOR linewidth. The hfc was found to be in excellent agreement with the best value of $|0.274|$ mT from the fit of the ^{17}O broadening in the cw-EPR of the Ras(wt)•Mn^{2+}•GDP complex (Table 4) and provided strong support for our previous cw-EPR results that in liquid solution only three water molecules are ligated to the metal ion.
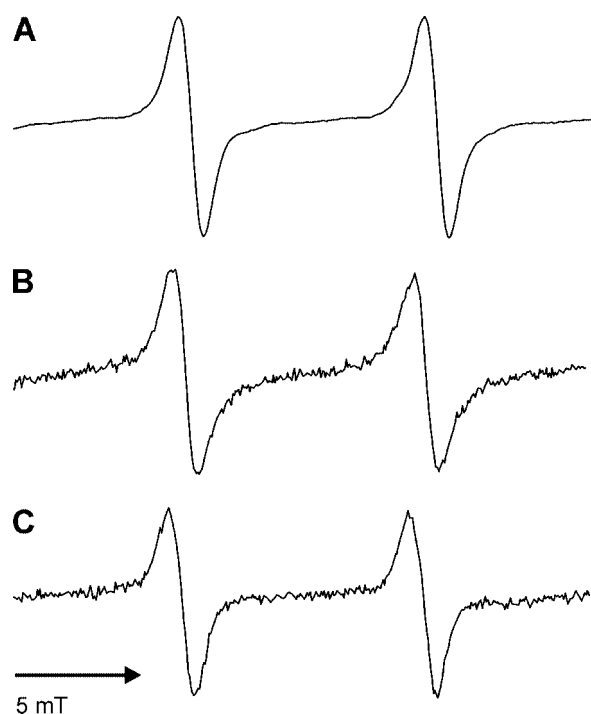
Comparison of the ligand sphere of Ras(wt)•Mn^{2+}•GDP and Ras(G12V)•Mn^{2+}•GDP complexes in frozen solution

Further ^{13}C and ^{31}P ENDOR experiments were performed to find more evidence for differences in the ligand sphere between the Ras(wt) and the oncogenic mutant Ras(G12V) bound to Mn^{2+}•GDP as revealed by the EPR analysis in liquid solution.[33] Consideration of the biochemical and physical properties of the Mn^{2+} centre in Ras had lead to the hypothesis that the missing ligand in Ras(wt)•Mn^{2+}•GDP could be either an amino acid or a phosphate ion. ^{13}C ENDOR was carried out on uniformly labelled and ^{13}C–Asp selectively labelled proteins.[41] The latter experiment was motivated by the earlier report from Schlichting *et al.*[4] that Asp57 is additionally coordinated by the side chain carboxyl group to the metal ion and by the proposal[33] that such a coordination pattern may be preserved for the wild-type protein complex in solution. However, the ^{13}C ENDOR spectra in frozen solution did not reveal any differences between the wild type and the G12V protein, and no large hfc to the ^{13}C of Asp57 could be observed. Additional careful evaluation of the ENDOR effect and comparison with the ^{13}C ENDOR spectra of the Ras(wt)•Mn^{2+}•GppNHp•effector complex, where the Thr35 is a further ligand to the metal ion, unambiguously indicated that in the frozen solutions of Ras(wt)•Mn^{2+}•GDP and Ras(G12V)•Mn^{2+}•GDP only one amino acid, i.e. the Ser17, is ligated to the metal ion.
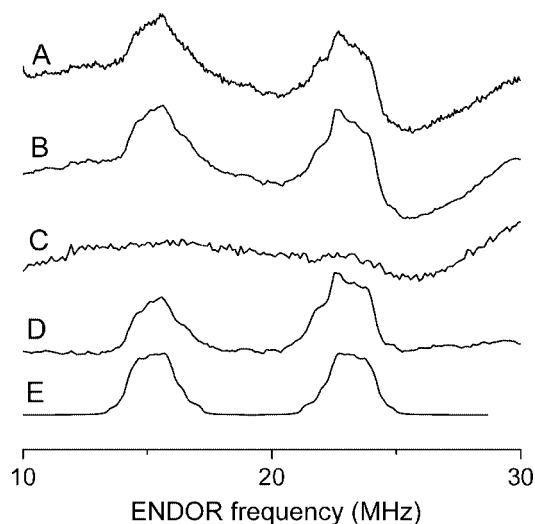
Figure 7. ^{17}O Davies ENDOR spectra of Ras(G12V)•Mn^{2+}•GDP and Ras(wt)•Mn^{2+}•GDP. The samples contained approximately 1 mM Ras(G12V)•Mn^{2+}•GDP (A) or Ras(wt)•Mn^{2+}•GDP (B) in 40 mM Hepes pH 7.4, 2 mM DTE. ^{17}O Davies ENDOR spectra were measured on one of the six hyperfine lines of the EPR $m_s = +1/2$ to $-1/2$ transition. For comparison, spectrum (C) was recorded outside the resonance of the sextet. The subtraction of spectrum (B) from (C) leads to spectrum (D), which shows the contribution of the EPR $m_s = +1/2$ to $-1/2$ transition. (E) Simulation of spectrum (D) with the parameters given in the text. Experimental parameters: (A) MW inversion pulse $t_\pi = 180$ ns, $t_{\pi/2} = 100$ ns, $t_\pi = 140$ ns, $\tau = 250$ ns, $t_{RF} = 22$ μs, shot repetition time = 25 ms, 45 scans with 10 shots per point. (B) Similar to (A) but with $t_\pi = 160$ ns, $\tau = 200$ ns, 15 scans with 20 shots per point. (C) Similar to (A) with 20 scans.

To further examine whether the missing ligand in the wild-type Ras•GDP complex could be a phosphate

ion, the ^{31}P ENDOR spectra of the Ras(wt)•Mn^{2+}•GDP, Ras(G12V)•Mn^{2+}•GDP, and Ras(wt)•Mn^{2+}•GppNHp•effector were compared.[41] Again, the ENDOR spectra of Ras(wt) and Ras(G12V) bound to Mn^{2+}•GDP were identical and could be well simulated with the contributions of one phosphorus with large hfc (the β-^{31}P of GDP) and one with a small hfc (the α-^{31}P of GDP). Instead, the complex of Ras(wt)•Mn^{2+}•GppNHp• with the RBD effector Raf-kinase showed two directly coordinated phosphate groups, the β- and γ-, and one weakly coupled phosphorus, the α-^{31}P. The results strongly suggested that, in frozen solution, Ras(wt)•Mn^{2+}•GDP and Ras(G12V)•Mn^{2+}•GDP do not differ in the number of coordinated phosphate groups.

CONCLUSIONS

Ras exists in several structural substates ('excited' states), which are not visible in the available crystal structures. There is a wealth of spectroscopic evidence from nuclear and electron magnetic resonance for their existence. They are spectroscopically well characterised. However, one has to be careful when discussing them since the conformational equilibria are easily shifted by perturbations such as point mutations of Ras itself and substitution of GTP analogs bound to Ras. Therefore, it is not necessarily true that a conformational state that is observed at room temperature in the liquid state is still dominant in the frozen or crystalline state or at very low temperatures.

Table 4. Number of water molecules and superhyperfine coupling constants coordinated to manganese in Ras−nucleotide complexes[a]

Ras complex	T (K)	Method	N	$\|A_{iso}\|$ (mT)
H-Ras(wt)•Mn^{2+}•GDP	297	EPR (95 GHz)[b]	3	0.27
H-Ras(wt)•Mn^{2+}•GDP	20	EPR (95 GHz)	4	0.28
	20	ENDOR (95 GHz)	−	0.276
N-Ras(wt)•Mn^{2+}•GDP	180	EPR (139 GHz)[c]	4	0.25
H-Ras(T35S)•Mn^{2+}•GDP	297	EPR (95 GHz)[b]	3	0.28
H-Ras(T35A)•Mn^{2+}•GDP	297	EPR (95 GHz)[b]	4	0.26
H-Ras(G12V)•Mn^{2+}•GDP	297	EPR (95 GHz)[b]	4	0.25
	20	ENDOR (95 GHz)	−	0.276
H-Ras(G12V/A59T)•Mn^{2+}•GDP	273	EPR (35 GHz)[d]	4	−
H-Ras(A59T)•Mn^{2+}•GDP	273	EPR (35 GHz)[d]	4	−
H-Ras(G12R/A59T)•Mn^{2+}•GDP	273	EPR (35 GHz)[d]	4	−
H-Ras(wt)•Mn^{2+}•GppNHp	20	EPR (95 GHz)	2	0.28
N-Ras(wt)•Mn^{2+}•GppNHp	180	EPR (139 GHz)[c]	2	0.28

[a] N, number of water ligands; A_{iso} isotropic part of the ^{17}O-^{55}Mn hyperfine coupling.

[b] Data from Rohrer *et al.*[33]

[c] Data from Bellew *et al.*,[31]; sample contained 15% methyl α-D-glucopyranoside as cryoprotectant.

[d] Data from Smithers *et al.*[50]; sample contained *N*-octyl β-D-glucopyranoside as cryoprotectant.

REFERENCES

1. Colicelli J. *Sci. STKE* 2004; **250**: 13.
2. Wittinghofer A, Waldmann H. *Angew. Chem. Int. Ed. Engl.* 2000; **39**: 4192.
3. Tong L, de Vos AM, Milburn MV, Kim SH. *J. Mol. Biol.* 1991; **217**: 503.
4. Schlichting I, Almo SC, Rapp G, Wilson K, Petratos K, Lentfer A, Wittinghofer A, Kabsch W, Pai EF, Petsko GA, Goody R. *Nature* 1990; **345**: 309.
5. Pai EF, Krengel U, Petsko GA, Goody RS, Kabsch W, Wittinghofer A. *EMBO J.* 1990; **9**: 2351.
6. Milburn MV, Tong L, de Vos AM, Brünger A, Yamaizumi Z, Nishimura S, Kim S-H. *Science* 1990; **247**: 939.
7. Scheidig AJ, Burmester C, Goody RS. *Structure* 1999; **7**: 1311.
8. Pai EF, Kabsch W, Krengel U, Holmes KC, John J, Wittinghofer A. *Nature* 1989; **341**: 209.
9. Scheffzek K, Ahmadian MR, Kabsch W, Wiesmuller L, Lautwein A, Schmitz F, Wittinghofer A. *Science* 1997; **277**: 333.
10. Geyer M, Schweins T, Herrmann C, Prisner T, Wittinghofer A, Kalbitzer HR. *Biochemistry* 1996; **35**: 10 308.
11. Ito Y, Yamasaki K, Iwahara J, Terada T, Kamiya A, Shirouzu M, Muto Y, Kawai G, Yokoyama S, Laue ED, Wälchi M, Shibata T, Nishimura S, Miyazawa T. *Biochemistry* 1997; **36**: 9109.
12. Hu JS, Redfield AG. *Biochemistry* 1997; **36**: 5045.
13. Spoerner M, Herrmann C, Vetter IR, Kalbitzer HR, Wittinghofer A. *Proc. Natl. Acad. Sci. USA* 2001; **98**: 4944.
14. Spoerner M, Wittinghofer A, Kalbitzer HR. *FEBS Lett.* 2004; **578**: 305.
15. Spoerner M, Nuehs A, Ganser P, Herrmann C, Wittinghofer A, Kalbitzer HR. *Biochemistry* 2005; **44**: 2225.
16. Cheng H, Sukal S, Deng H, Leyh TS, Callender R. *Biochemistry* 2001; **40**: 4035.
17. Allin C, Ahmadian MR, Wittinghofer A, Gerwert K. *Proc. Natl. Acad. Sci. USA* 2001; **98**: 7754.
18. Allin C, Gerwert K. *Biochemistry* 2001; **40**: 3037.
19. Du X, Frei H, Kim SH. *J. Biol. Chem.* 2000; **275**: 8492.
20. Wang JH, Xiao DG, Deng H, Webb MR, Callender R. *Biochemistry* 1998; **37**: 11106.
21. Futatsugi N, Tsuda M. *Biophys. J.* 2001; **81**: 3483.
22. Ma J, Karplus M. *Proc. Natl. Acad. Sci. USA* 1997; **94**: 11 905.
23. Glennon TM, Villà J, Warshel A. *Biochemistry* 2000; **39**: 9641.
24. Reed GH, Markham GD. *Biol. Magn. Reson.* 1984; **6**: 73.
25. Latwesen DG, Poe M, Leigh JS, Reed GH. *Biochemistry* 1992; **31**: 4946.
26. Haller M, Hoffman U, Schanding T, Goody RS, Vogel PD. *J. Biol. Chem.* 1997; **272**: 30103.
27. Halkides CJ, Farrar CT, Larsen RG, Redfield AG, Singel DJ. *Biochemistry* 1994; **33**: 4019.
28. Halkides CJ, Farrar CT, Singel DJ. *J. Mag. Res.* 1998; **134**: 142.
29. Farrar CT, Ma J, Singel DJ, Halkides CJ. *Structure* 2000; **8**: 1279.
30. Prisner TF, Rohrer M, Möbius K. *Appl. Magn. Reson.* 1994; **7**: 167.
31. Bellew BF, Halkides CJ, Gerfen GJ, Griffin RG, Singel DJ. *Biochemistry* 1996; **35**: 12186.
32. Halkides CJ, Bellew BF, Gerfen GJ, Farrar CT, Carter PH, Ruo B, Evans DA, Griffin RG, Singel DJ. *Biochemistry* 1996; **35**: 12194.
33. Rohrer M, Prisner TF, Brügmann O, Käss H, Spoerner M, Wittinghofer A, Kalbitzer HR. *Biochemistry* 2001; **40**: 1884.
34. Schweins T, Scheffzek K, Aßheuer R, Wittinghofer A. *J. Mol. Biol.* 1997; **266**: 847.
35. Tucker J, Sczakiel G, Feuerstein J, John J, Goody RS, Wittinghofer A. *EMBO J.* 1986; **5**: 1351.
36. Herrmann C, Martin GA, Wittinghofer A. *J. Biol. Chem.* 1995; **270**: 2901.
37. Herrmann C, Horn G, Spaargaren M, Wittinghofer A. *J. Biol. Chem.* 1996; **271**: 6794.
38. Shaka AJ, Baker PB, Freeman R. *J. Magn. Reson.* 1985; **64**: 547.
39. Maurer T, Kalbitzer HR. *J. Magn. Reson.* 1996; **B113**: 177.
40. Raiford DS, Fisk CG, Becker ED. *Anal. Chem.* 1979; **51**: 2050.
41. Bennati M, Hertel MM, Fritscher J, Prisner TF, Weiden N, Dinse K-P, Hofweber R, Spoerner M, Horn G, Kalbitzer HR. *Biochemistry* submitted.
42. Stumber M, Geyer M, Kalbitzer HR, Scheffzek K, Haeberlen U. *J. Mol. Biol.* 2002; **323**: 899.
43. Iuga A, Spoerner M, Kalbitzer HR, Brunner E. *J. Mol. Biol.* 2004; **342**: 1033.
44. Mehring M. *Principles of High Resolution NMR in Solids*. Springer: Berlin, 1983.
45. Geyer M, Herrmann C, Wohlgemuth S, Wittinghofer A, Kalbitzer HR. *Nat. Struct. Biol.* 1997; **4**: 694.
46. Linnemann T, Geyer M, Jaitner BK, Block C, Kalbitzer HR, Wittinghofer A, Herrmann C. *J. Biol. Chem.* 1999; **274**: 13556.
47. Gronwald W, Huber F, Grünewald P, Spörner M, Wohlgemuth S, Herrmann C, Kalbitzer HR. *Structure* 2001; **9**: 1029.
48. John J, Rensland H, Schlichting I, Vetter I, Borasio GD, Goody RS, Wittinghofer A. *J. Biol. Chem.* 1993; **268**: 923.
49. Schweins T, Geyer M, Scheffzek K, Warshel A, Kalbitzer HR, Wittinghofer A. *Nat. Struct. Biol.* 1995; **2**: 36.
50. Smithers GW, Poe M, Latwesen DG, Reed GH. *Arch. Biochem. Biophys.* 1990; **280**: 416.
51. Kalbitzer HR, Goody RS, Wittinghofer A. *Eur. J. Biochem.* 1984; **141**: 591.
52. Bennati M, Farrar CT, Bryant JA, Inati SJ, Weis V, Gerfen GJ, Riggs-Gelasco P, Stubbe J, Griffin RG. *J. Magn. Reson.* 1999; **138**: 232.
53. Epel B, Pöppl A, Manikandan P, Vega S, Goldfarb D. *J. Magn. Res.* 2001; **148**: 388.
54. Tan X, Bernardo M, Thomann H, Scholes CP. *J. Chem. Phys.* 1995; **102**: 2675.